Surface science insight note: Optimizing XPS instrument performance for quantification of spectra

Vincent Fernandez, Olivier Renault, Neal Fairley, Jonas Baltrusaitis

Surface Science Insight Note: Optimizing XPS Instrument Performance for Quantification of Spectra

Vincent Fernandez[1], Olivier Renault,[2] Neal Fairley,[3] and Jonas Baltrusaitis[4,*]

1 Institut des Matériaux Jean Rouxel (IMN), UMR-6502 CNRS, Université de Nantes, 2 rue de la Houssinière, BP32229, 44322 Nantes cedex 3, France

2 Univ.Grenoble Alpes, CEA, LETI, F-38000 Grenoble, France.

3 Casa Software Ltd, Bay House, 5 Grosvenor Terrace, Teignmouth, Devon TQ14 8NE, UK

4 Department of Chemical and Biomolecular Engineering, Lehigh University, 111 Research Drive, Bethlehem, PA 18015, USA

Abstract

X-ray Photoelectron Spectroscopy (XPS) provides quantitative information from photoemission peaks and shapes observed within the background due to the inelastic scattering of photoelectrons. To quantify the signal, both photoemission peaks and background in spectra must be adjusted for instrumental transmission variations that are a consequence of changes in efficiency when recording electrons with different kinetic energy. While it is generally assumed that correcting spectroscopic data for transmission is a necessary part of quantification by XPS, there are consequences for the quantification of spectra measured using an instrument for which transmission has significant curvature. In this *Insight*, the implications of curvature in transmission characteristics are discussed and a method based on XPS microscopy is proposed that ensures the transmission response of an instrument is free from significant curvature. An example of an instrument for which a flat transmission response is presented is achieved through collecting spectra using lens modes designed to measure stigmatic images.

*corresponding author: job314@lehigh.edu; +1-610-758-6836

Keywords: XPS, imaging, aberration, quantification

Introduction

Understanding surface chemistry is of paramount importance in materials for energy, including solar cells, battery technology and heterogeneous catalysis during their evolution, degradation and regeneration. X-ray Photoelectron Spectroscopy (XPS) is an essential surface analysis technique since it is quantitative in terms of elemental composition and chemical environment [1]–[3]. For homogeneous flat samples, the relative amounts for two elements are proportional to the peak area ratio [4] and the relative uncertainties are inversely proportional to measuring time squared [5]. In theory, there is no limitation to quantification accuracy. In practice, ionization cross-sections [6], experiment geometry, instrument stability, sample desorption, non-linearity of the detector, variation with the kinetic energy of the Effective Attenuation Length EAL [7], analyzer transmission function [4], [8]–[12], statistics [13] and accurate background determination [14]–[16] limit the quantification accuracy. Photoemission peak intensity is converted to the amount of substance by dividing each peak area by a factor specific to each photoemission line. In theory, it is quite clear how these factors are derived. In practice, theoretical partitioning into distinct mechanisms underlying these scaling factors is less clear.

For practical reasons relating to the measurement of electrons with specific kinetic energy, transmission correction is a necessary part of quantifying XPS data. Specifically, each XPS instrument must be configured for use and therefore the performance of different instruments may differ. More importantly, different instrument designs place different emphasis on the desired outcomes for an analysis. The most obvious examples are instruments aimed at ambient pressure XPS compared to instruments designed to measure angular resolved spectra. In any event, the energy analyser of an XPS instrument accepts electrons of an energy determined by the, so called, pass energy. That is, only electrons close in energy to the pass energy are permitted to enter the detectors. Since an energy spectrum is measured over a wide range of energies and XPS is performed using a constant pass energy, XPS instruments must retard photoelectrons with initial kinetic energy greater than the pass energy of the analyser. Consequentially, electrostatic and/or magnetic lenses used to present photoelectrons at the entrance to the energy filter must scan voltages during measurement of a spectrum. Lenses that perform the role of guiding photoelectrons to the energy analyser are arranged sequentially in a column between the sample and the entrance to the energy analyser. Further, electron optics dictates that apertures separating lenses are a necessary part of achieving, when measuring spectra, optimum count-rate for optimum energy resolution. Therefore, the collective influence of lenses and apertures is referred herein as the analyser lens-column. The design of the analyser lens-column, the implementation of lens voltages and the size and position of apertures in the analyser lens-

column cause variation in sensitivity for an instrument throughout the measurement of a spectrum, and these variations in sensitivity must be characterised to permit accurate quantification. There is no widely accepted procedure for calculating the transmission for commercially available instruments. In theory, all instruments can be used to quantify a sample by following the same procedure. The mere fact that quantification procedures between instruments of different designs rely on different sets of relative sensitivity factors (RSFs) suggests a problem exists. Since transmission correction is associated with instrument design, computing transmission functions for an instrument represents an obvious source of error which is rectified by adjustments to RSFs.

Historically, there have been two approaches to the quantification of XPS spectra. The first approach involves the creation of RSFs calculated using standard materials to assess the relative intensity of photoemission peaks from materials with known stoichiometry measured from a specific instrument and operating mode. Other operating modes and other instruments make use of these RSFs by calculating transmission functions which describe variation in intensity as a function of kinetic energy relative to the instrument for which RSFs are determined. When measured empirically, RSFs necessarily include some characteristics related to the considered instrument and to the reference samples such as Teflon-PTFE, PET, SiO_2 or LiF used to create the RSF database step-by-step. In particular, since removing the contribution of transmission variations from these empirical RSFs requires a reliable means of determining an absolute transmission function for instruments used to measure standard samples, errors in computing the transmission function necessarily contribute to uncertainty in these RSFs. Traceability in terms of corrections applied to photoemission peak area is compromised if these RSF databases do not include information related to background approximation used to compute photoemission peak areas for each RSF together with specific instrumental configuration and properties used to measure spectra.

An alternative approach is to calculate the true spectrometer transmission function of the considered instrument [11]. Access to such a true (or absolute) transmission function opens the possibility of separate corrections to photoemission intensity based on computed photoionization cross-sections, adjusted for angular distribution corrections to account for instrument geometry of X-ray source and analyzer lens-column and finally, escape depth corrections to account for attenuation of photoemission signal at different kinetic energies due to inelastic scattering. In the past, a true transmission function was derived using clean gold, copper and silver samples to characterize the analyzer [4]. Other attempts to derive true transmission include the use of a reference sample with many core levels to create an absolute transmission function [17], the use of background to polymers or the use of background to a reference gold spectrum to characterize instrument transmission [9].

Another approach is to use an electron gun to characterize the surface analyzed as a function of the kinetic energy and use the answer to create a true transmission function [10] . The use of theoretically determined corrections as part of quantification, while potentially imperfect, provides a starting point from which to make assertions about results obtained for a sample. Computing a true transmission function from spectra involves fitting functional forms to data containing noise. When fitting functional form to data, low signal-to-noise becomes increasingly an issue that is difficult to avoid for low-sensitivity instrumental modes. Further, attempting to fit transmission characteristics with a single curve, complex transmission response of an instrument is also a cause of mathematical concern, hence there is value in ensuring the true transmission response of an instrument is as simple a curve as possible.

An alternative approach described in this *Insight Note* is to identify instrumental operating modes for which transmission correction is unnecessary or as simple as possible. Central to this approach is the use of stigmatic images to characterize an instrument and present a photoemission signal for energy analysis representative of the signal leaving the sample independent of initial electron energy. The principal point for this approach is the analysis area defined by the lens optical column remains constant for all photoemission energies used in spectroscopic mode.

Assuming bulk homogeneous samples allows transmission correction to include variation in the analysis area as a function of kinetic energy. The analysis area may vary for several reasons including changes in analysis area as a function of kinetic energy due to imperfect lens tuning or physical limitations to signal transfer resulting from mismatch of lens optics and apertures within the lens column. The use of stigmatic imaging lens modes, also used for spectroscopic measurements, identifies and allows corrections to lens optics that limit the influence of these imperfections on spectra. In this *Insight Note*, we report two operating modes that offer near-flat transmission response. Comparison with a stigmatic imaging XPS instrument of different designs further demonstrates the importance of stigmatic imaging even though in this second example the stigmatic image is transformed by a Fourier lens before the entrance of the hemispherical analyzer (HSA). The similarity and significant feature of these stigmatic imaging instruments is the possibility of ensuring a spectrum representative of a specific location on a sample. The concept of keeping the same area analyzed irrespective of kinetic energy is important, for example, since charge compensation or X-ray flux performance may differ across a surface. Primarily, however, constant area analyzed for all energies is necessary for investigating samples that are laterally inhomogeneity and/or inhomogeneous with depth. In this *Insight Note*, we consider the influence of instrument design on quantification by XPS by considering how stigmatic

imaging XPS instruments can be used to understand and optimize transmission performance across energy ranges typical for laboratory-based analysis. Optimal instrument performance is achieved by maintaining the same surface and the same angular acceptance. Following an instrumental approach, the need for transmission is simplified or eliminated from the steps required for traceable quantification.

Experimental

Measurements were performed using a Kratos Axis Ultra, a Kratos Axis Nova (both Spherical Mirror Analysers) and a NanoESCA spectromicroscope from ScientaOmicron equipped with a Dual Hemispherical Analyser Fourier Transform [18], [19].

Spherical Mirror Analyser (SMA)

Monochromatic Al Kα X-ray source power was between 45 and 300 Watts. Low power on clean metallic samples was used to avoid detector saturation. The X-ray source was started at least 30 min before sample measurement to ensure good X-ray spot stability during the measurements.

Both Kratos instruments are equipped with two-dimensional delay line detectors (DLD) used for both imaging and spectroscopy [18]. Kratos instruments are designed with two Hemispherical Analysers (HSAs) [20], [21] arranged to allow the use of the same DLD to record spectra and images and with coincident entrance apertures. The larger radius HSA operates as an SMA [21], [22] capable of transferring an energy-filtered image of the sample formed at the entrance aperture to the exit aperture with a magnification of -1. The smaller radius HSA operates in deflection mode and is used to create energy dispersed signal across the DLD functioning as a linear multiple-channel detector. The arrangement of these dual analyzers is useful for making use of the same lens mode for imaging and spectroscopy. Two values of pass energy (PE) were used to acquire spectra, namely, PE 160 and PE 80. Each of these two pass energies is tuned independently using different tables of lens voltages for tuning image quality at a range of emission energies. For optimal transmission characteristics, Field of View (FoV2) was used. In FoV2, spectra and images are acquired using the imaging lens mode capable of transferring an image of the sample from an area at the sample of size 450 microns by 450 microns. In spectroscopy mode, a slot aperture is used at the entrance to the dual analyzer of width approximately one-third of the analysis area, whereas in imaging mode the entrance is essentially open to allow an image of spatial dimensions 450 microns by 450 microns to be recorded using the DLD operating as a two-dimensional detector. PE 160 FoV2 does not produce the most sensitivity but it will be considered a good compromise between stability and sensitivity operating mode for a Kratos instrument.

By contrast to FoV2, hybrid mode PE160 on a Kratos Axis Ultra is designed to optimize sensitivity. The analysis area at the sample is expected to be 800 microns by 300 microns and the acceptance angular cone at the sample is designed to alter with kinetic energy to optimize the number of electrons detected. These characteristics of the hybrid mode ensure a transmission function is not uniformly constant concerning the kinetic energy but does provide the most sensitive mode for a Kratos Axis Ultra. Both Kratos Axis Ultra and Kratos Axis Nova offer FoV2 however the Kratos Axis Nova does not offer hybrid mode.

Making use of FoV2 and the SMA it is possible to compare image characteristics using a gold grid and measuring images for kinetic energies equivalent to background intensity generated by gold photoemission peaks. Figure 1 is an overlay of three images measured from a gold grid using kinetic energies at the extremes of 86 and 1136 eV used to acquire a typical survey spectrum and one kinetic energy in the middle of 736 eV.

The lens column for both Kratos instruments is illustrated in Figure 2. Image quality is altered using the angular acceptance iris shown in Figure 2 and all imaging measurements were performed with the angular acceptance iris closed (minimum diameter) to achieve the highest possible resolution image. The mode FoV2 PE 160eV is the best in terms of FoV size stability, image center stability, and spatial resolution quality independent of the kinetic energy and intensity. Achieving these image characteristics is accomplished by adjustments to lens functions used to generate lens voltages for measurement at specific kinetic energy. The surface analyzed stabilities were optimized between kinetic energies 350 eV and 1484 eV. The importance of correctly tuning a particular lens within the lens column depicted in Figure 2 is illustrated in Figure 3, where overlaid images of a gold grid demonstrate possible deformations in images due to incorrect tuning of a lens referred to as the lens V6 for a single node in the lens function corresponding to kinetic energy 900 eV. The lens function for V6 is defined using lens nodes for kinetic energies 0, 100, 350, 600, 900, 1169, 1500 and 5000 eV. Lens voltages between nodes are obtained by linear interpolation. The sequence of images in Figure 3 shows how scanning the voltage on lens V6 for one node at kinetic energy 900 eV results in increased magnification for lower voltage compared to the optimum voltage and a decrease in magnification for voltages greater than optimum. The changes in image size and quality translate into lens modes that influence spectroscopic mode as shown in Figure 4 where clean bulk gold is measured for each perturbation to the V6 voltage at the node with kinetic energy 900 eV.

Survey spectra used to characterize transmission for these instruments are measured in the 350-1500 eV kinetic energy range. Homogeneous silver and gold foil samples were cleaned using an ion beam to remove evidence of carbon and oxygen before measuring spectra.

Spectral data acquired on the Kratos Axis Nova made use of FOV2 PE160 eV with open angular acceptance and an analysis area at the sample of 150 microns x 500 microns. Figure 5 illustrates a survey gold spectrum measured under these operating conditions using the Axis Nova.

Experiments were performed to assess the influence of the angular acceptance iris (Figure 2) using FOV2 PE 80 eV on the Axis Ultra. Figure 6 illustrates the loss of signal associated with using the angular acceptance iris fully open and fully closed. Closing the angular acceptance iris results in a reduction in intensity by a factor of about seven compared to the same iris fully open. However, the transmission behavior resulting from altering the angular acceptance iris is identical which is demonstrated by the ratio plot for the two spectra in Figure 6A shown in Figure 6B. When spectra are acquired in spectroscopic mode using FoV2 and PE 160 or PE 80, the overall energy resolution at these pass energies and slot aperture filled by signal at the entrance to the HSA measured on Ag $3d_{5/2}$ is about 1.9 eV and 0.95 eV, respectively.

Dual Hemispherical Analyser Fourier Transform

The NanoESCA combines a Photoemission Electron Microscope (PEEM) with a spectrometer in the form of two HSAs designed to provide high transmission in XPS imaging. Therefore the instrument allows energy-resolved core-level images of a sample with a best lateral resolution of 650 nm [18], [19] and the resolution of secondary electron images (providing work function information) to be typically better than 100 nm. One of the big advantages of the instrument is the perfect control of the analysis area, due to the very high instrumental lateral resolution of the PEEM and optimal image transmission through the spectrometer. The PEEM column creates and magnifies an image of the sample surface by a combination of an electrostatic immersion objective and a set of projective electrostatic lenses, which is further transmitted and energy-filtered by the double-HSA spectrometer. The objective lens enables collecting photoelectrons over a large solid angle (25-90°) which depends on the inverse of the kinetic energy and is further reduced by a contrast aperture (CA). The CA, located in the back-focal plane of the objective lens, and used to improve the lateral resolution by reducing the aberrations of the objective lens, further decreasing the maximal electron emission angle, and concomitantly, the overall PEEM transmission. In most situations, the CA diameter determines the angular phase space in the instrument, i.e., the angle reduction by the CA is transferred to the spectrometer entrance plane.

For the experiments, two data sets were collected with identical conditions from sputtered clean gold except for the CA setting. The survey spectra (786.6-1486.6 eV kinetic energy, 0.5 eV/step) were recorded in energy-filtered mode (one image per energy) with the multi-

channel plate detector in event-counting mode, at pass energy of 50 eV and a 1 mm entrance slit and with a CA diameter of either 1500 and 500 μm. These data were measured using Al Kα monochromatic X-rays.

Comparison of both instruments

The characteristics common to both SMA and NanoESCA instruments are well-focused, well-registered images of a specific location on a sample achieved. A necessary condition is therefore met for good transmission response. A difference between lens optics of the NanoESCA and the Kratos Axis is that the NanoESCA method of electron collection over a range of angles concerning the sample normal, which is performed with an electrostatic objective lens that in principle alters the angular acceptance as the inverse of the electron kinetic energy. Kratos Axis performs the gathering of these same electrons using a magnetic lens. Another difference between the NanoESCA and the Kratos Axis is that the analysis area at the sample forms (in the case of the NanoESCA) an image as input to a Fourier lens offset from the first HSA entrance aperture. The Fourier lens is used to convert spatial and angular information into angular and spatial information for acceptance to the HSA. This is in contrast to the Kratos Axis lens column for which the HSA acting as an SMA requires a spatially resolved image to be formed with near paraxial electrons to the normal of the image plane at the entrance to the SMA precisely at the entrance to the HSA. For the NanoESCA the photoelectron solid angle emitted from the sample and then transmitted through the PEEM column is determined by a contrast aperture (CA) located in the back focal plane of the objective lens. The diameter of the contrast aperture is expected to alter transmission behavior for the NanoESCA. The equivalent aperture to the NanoESCA CA in an Axis instrument is the angular acceptance iris.

Relative Sensitivity, Angular Distribution and Escape Depth Correction

All data analysis and manipulation were performed using CasaXPS version 2.3.23 [24]. Photoemission peaks are scaled using Scofield cross-sections to allow for intensity variation for different elements and electron configurations. For an Axis Nova, the angle between the X-ray source and the axis of the lens system is the so-called magic angle, for which angular distribution considerations for photoemission intensity variation can be neglected. We also present results comparing photoemission from core levels with *s* symmetry for which angular distribution correction is identical and independent of element or core level.

Quantification by XPS requires an escape depth adjustment to the photoemission signal. The results presented in this *Insight Note* assume a bulk material and the use of the universal formula for effective attenuation length Equation [1].

$$EAL = \frac{\left(0.65+0.007E^{0.93}\right)}{Z^{0.38}} \quad (nm) \qquad [1],$$

Where E is the kinetic energy for a photoelectron and Z is the mean atomic number of the material analyzed [23].

Results and Discussion

Figure 7 presents gold survey spectra acquired from the Kratos Axis Nova using FOV2 PE 160 eV and FOV2 PE 80 eV to a gold spectrum measured from a Kratos Axis Ultra hybrid mode PE 80 [11] after correction for true transmission using the approach described by Cumpson *et al*. [25], hereafter referred to as NPL. Hybrid mode PE 80 provides ample count rate to permit a precise determination of transmission function by the NPL approach and we assert the NPL procedure applied to the data in Figure 7 is evidence data measured using FOV2 PE 160 eV and FOV2 PE 80 eV are true spectra from a clean gold sample free from significant transmission fluctuations. The explanation we propose for the instrumental property of constant transmission response for FOV2 PE 160 eV and FOV2 PE 80 eV is as follows.

Kratos Axis lens systems are designed to transfer electrons from a sample to the entrance aperture to the dual-mode hemispherical analyzer. The significant feature of this dual analyzer is the same lens system can be used to acquire spatially resolved energy-filtered signal via the SMA as is used to collect signal without spatial information via the spectroscopic deflection mode HSA. As a consequence of these imaging modes being available for collecting spectra as well as images, the criteria for tuning imaging lens modes allow the pre-selection of photoemission electrons for energy analysis by the deflection analyzer to be identical across the range of kinetic energies used when collecting spectra. The conditions required to form well-focused images at all kinetic energies are close to the conditions required for a flat response of the deflection analyzers when measuring spectra, namely, the sample area analyzed is identical for all electrons in a spectrum, electrons entering the hemispherical analyzer are near paraxial and therefore approach the ideal trajectory for transfer to the detection system and the response of signal intensity to restricting the angular acceptance iris is uniform across different kinetic energies. The combination of these characteristics leads to a flat transmission response for an instrument tuned to achieve well-formed and spatially registered images across kinetic energies used to acquire spectra.

Transfer lens modes for non-imaging applications are designed to collect all available electrons emitted from the sample. The objective is high sensitivity gained by taking advantage of a varying angular acceptance with kinetic energy, which is characterized by a transmission response to the kinetic energy of diminishing signal for increasing kinetic energy. Imaging lens modes perform a different task of restricting the influence of varying angular acceptance with kinetic energy and therefore act as a pre-filter limiting the angle of acceptance for electrons emitted from the surface for different kinetic energies that are allowed to enter the deflection HSA. We may therefore consider these imaging lens modes in terms of vector quantities, namely, a velocity filter for photoemission that leads to a flat transmission response to kinetic energy.

The contrast between the conditions required for the Kratos Axis SMA and the images acquired using a NanoESCA is shown in Figure 8. Gold spectra measured using two CA sizes are plotted relative to the NPL true gold spectrum. The expected kinetic energy dependence of transmission is obvious in Figure 8. The relative backgrounds indicate that the transmission response for the NanoESCA depends on the CA setting, which is not unexpected. The significance of these NanoESCA gold spectra relative to the NPL true gold spectrum is the well-behaved transmission response that can be modelled making use of a very simple energy power law. It also means that the analysis area is, as expected from the instrumental setup itself, identical over the entire energy interval used to collect the image series. The equivalent experiment performed on a Kratos Axis Ultra is performed by adjusting the angular acceptance iris. The difference between using a fully closed angular acceptance iris and a fully open setting for hybrid mode PE 80 compared to PE80 FoV2 is shown in Figure 9. Hybrid mode is designed for sensitivity which is achieved by making use of the magnetic lens to collect for large acceptance angles. Note how close the angular acceptance iris results in lower sensitivity in both cases, however, FoV 2 uniformly drops in sensitivity whereas hybrid sensitivity changes as a function of kinetic energy. These comparisons are seen as evidence that FoV 2 is performing consistently for all kinetic energies contributing to a flat transmission response.

Transmission-free spectra are of little value in terms of quantification unless it can be shown the use of Scofield cross-sections and effective attenuation length corrections are equally as valid. We choose to demonstrate the potential for traceable quantification by considering relative photoemission intensities for s-orbital peaks measured from sodium chloride. Sodium chloride offers three s-orbital peaks spread over a wide range of kinetic energies. Further, a band gap for NaCl ensures the background signal beneath these photoemission peaks due to these peaks being flat. Inelastic scattering of signal to higher kinetic energy is not flat, thus to estimate peak areas attributed to photoemission of Na 1s, Cl 2s and Na 2s the

backgrounds are determined by extrapolating the behavior of signal to higher kinetic energy relative to these photoemission peaks. Figure 10 illustrates a fit of Voigt line shapes to these photoemission peaks used to compute intensity by area which is adjusted using Scofield cross-sections to correct for differing emission probabilities. Inelastic scattering attenuates signal as a function of kinetic energy and these differences in expected peak intensity play an important role in quantification of NaCl. Assuming bulk homogeneous NaCl, the corrected %area for each peak in Figure 10 is computed using the EAL defined by Equation [1]. The line shape for Cl 2s is significantly more Lorentzian than both Na 1s and Na 2s, a point that is important in achieving the expected relationship for Na 1s, Na 2s and Cl 2s. A similar comparison between Cl 2s and Cl 2p based on an identical procedure for estimating Cl 2p similarly is within the expected 1:1 ratio after correcting using Scofield cross-sections and EAL.

We note at this point the conventional method for estimating peak area applied to isolated peaks is to use a background approximation alone to separate photoemission without energy loss from inelastic scattered background. If a Shirley background is used to define the photoemission signal the ratio for these Cl 2s and Cl 2p peaks is 1:1.2 compared to the ratio of 1:1.04 if estimated using Voigt line shapes as shown in Figure 11.

Conclusions

We have demonstrated how imaging lens modes used to acquire spectroscopic data can yield spectroscopic data without the need to perform transmission correction as part of quantification procedures. The importance of quantification by XPS of maintaining the same analysis area for all kinetic energies was discussed. An example of quantification for NaCl shows traceable quantification is attainable using Scofield cross-sections and effective attenuation length corrections. A flat transmission response achieved by tuning stigmatic images is possible for an energy interval from 350 eV kinetic energy up to and including the Fermi edge of gold. Quantification performed using escape depth correction and Scofield cross-sections only, demonstrated the efficacy of the procedure, in the sense that quantification compatible with sample knowledge is possible for spectra measured from an instrument tuned by the procedure as described. Uncertainty in these quantification results induced by analysis steps, escape depth correction and cross-sections are acknowledged, therefore these apparently accurate results, merely demonstrate that the absence of a transmission correction in computing relative proportions of photoemission peaks by the procedure described herein permits quantification with uncertainty that is limited by the uncertainties expected for quantification by XPS.

While not all instruments and operating modes can be made to follow the procedures used to create operating modes with flat transmission response, awareness of images within the formation of spectra offers a model for ensuring transmission response is simple. Simplicity for transmission response is critical to characterizing operating modes for which sufficient signal-to-noise is difficult to achieve.

A conclusion of interest for all instruments with variable-sized apertures located at a position equivalent to the angular acceptance iris indicated in Figure 2 is that transmission for such instruments is potentially sensitive to the size of this iris. If the performance of an instrument is dependent on varying solid angles accepted by the lens column with kinetic energy, it is important to quantify by XPS that a transmission function is determined and available for all operating modes that differ in angular acceptance iris setting.

Acknowledgments

This work by JB was supported as part of Understanding & Controlling Accelerated and Gradual Evolution of Materials for Energy (UNCAGE-ME), an Energy Frontier Research Center funded by the U.S. Department of Energy, Office of Science, Basic Energy Sciences under Award # DE-SC0012577. The CNRS is acknowledged for financial support to the Thematic Workshop (N° 1317144) held at the Station Biologique, Roscoff, France.

Author contributions

Vincent Fernandez: Investigation (lead); Writing – review and editing (equal); Writing – original draft (equal);. Olivier Renault: Investigation (lead); Writing – review and editing (equal); Writing – original draft (equal);. Neal Fairley: Conceptualization (lead); Investigation (supporting); Methodology (lead); Writing – original draft (equal); Writing – review and editing (equal). Jonas Baltrusaitis: Methodology (supporting); Supervision (lead); Writing – original draft (equal); Writing – review and editing (equal).

Competing interests

The authors declare no competing interests.

Figure 1. Overlay of gold grid measured at different binding energy using a monochromatic Al K alpha source. The white color corresponds to a perfect overlay of these 3 images. The measure was performed with a Kratos Nova instrument at PE 160 eV.

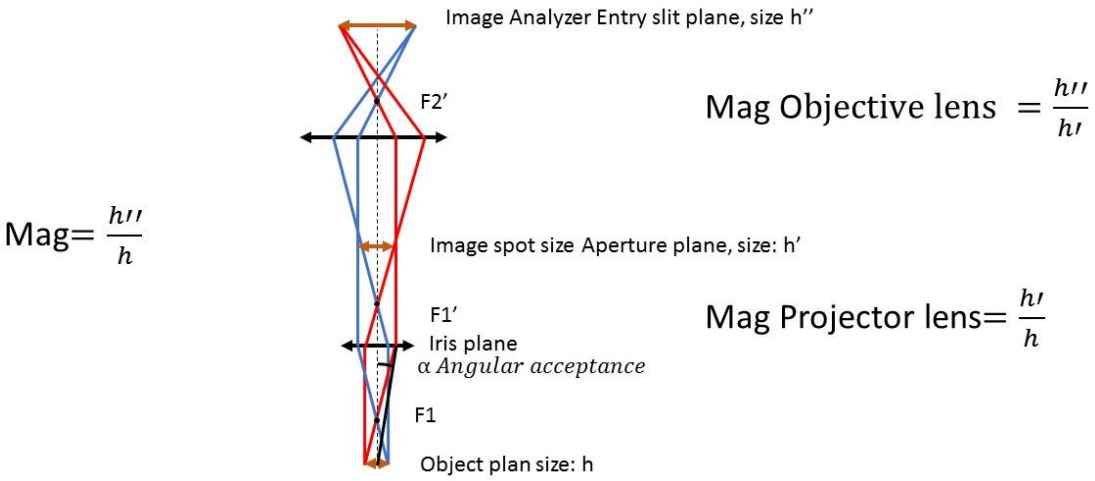

Figure 2. Diagram of the lens column for both Kratos Axis Ultra and Kratos Axis Nova.

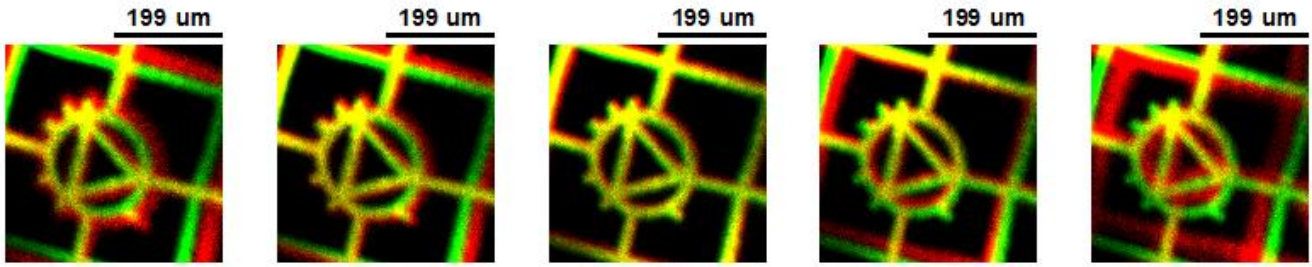

V6= 786V at Ke=900eV | V6= 796V at Ke=900eV | V6= 806V at Ke=900eV | V6= 816V at Ke=900eV | V6= 826V at Ke=900eV

Figure 3. Effect of the magnification objective lens V6 at 900eV on a gold grid sample image. The red image color corresponds to the grid image at KE=900 eV and the green image is the image formed for KE=1402 eV representing the reference image against which changes to V6 voltage are compared. Yellow is obtained for pixels where the overlay of the red and green are of equal intensity in the respective color scales.

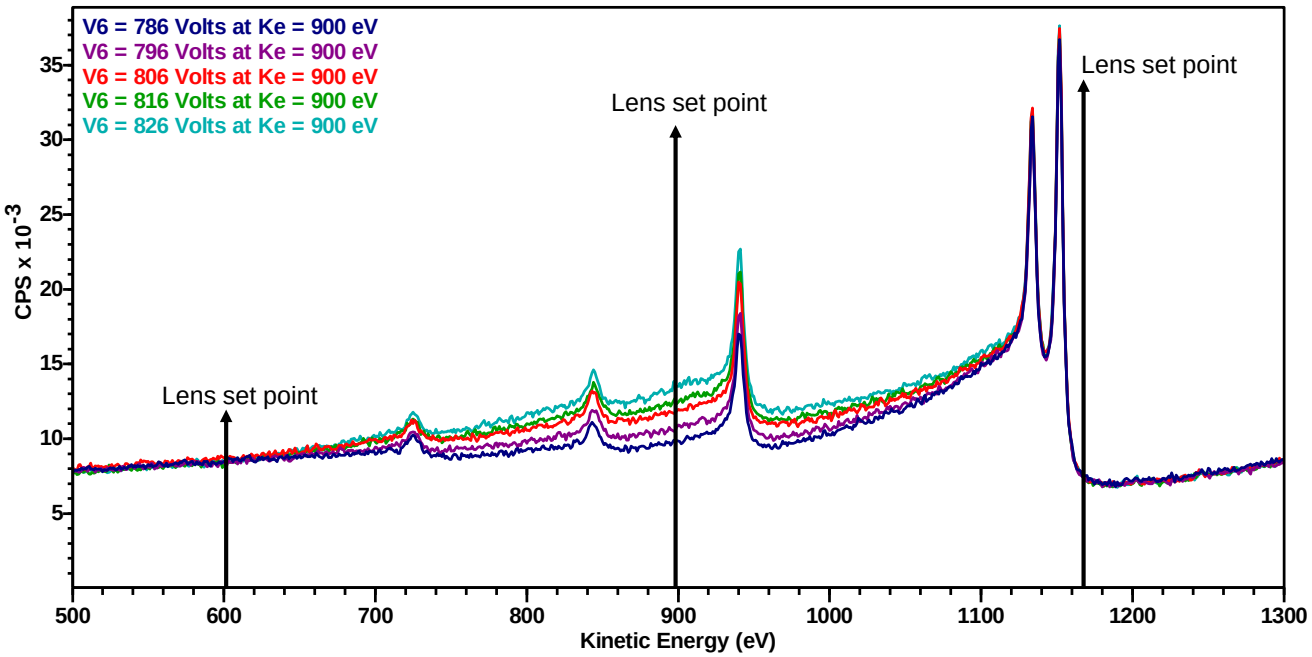

Figure 4 Influence of the magnification objective lens V6 at 900eV on a clean gold sample spectrum.

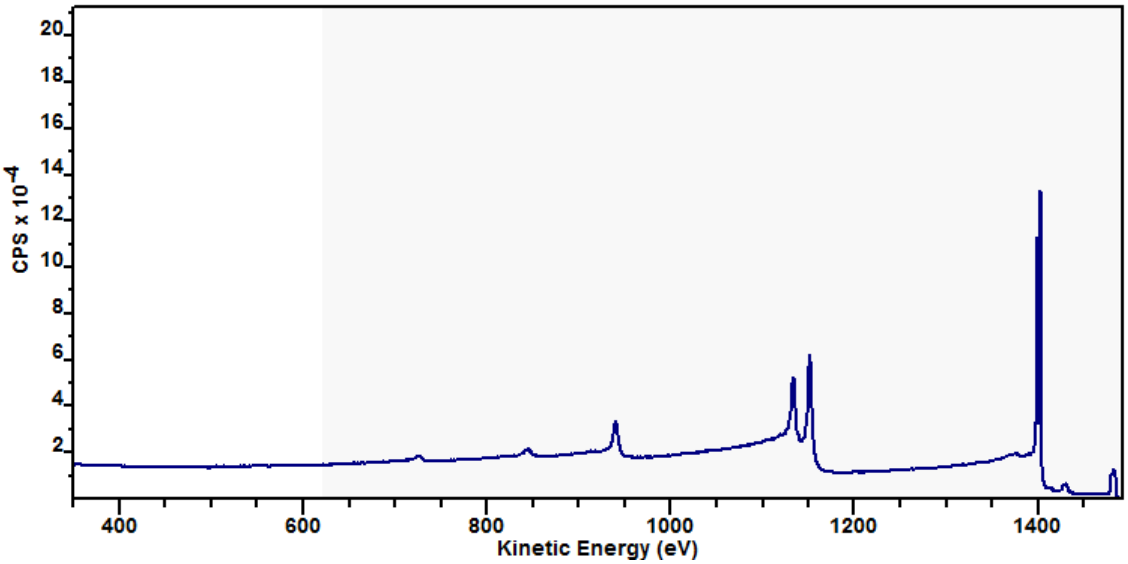

Figure 5. True gold spectrum between kinetic energy 350 and 1492 eV with a step of 0.4 using an FOV2 with a surface analyzed of 150 microns by 500 microns PE 160 eV.

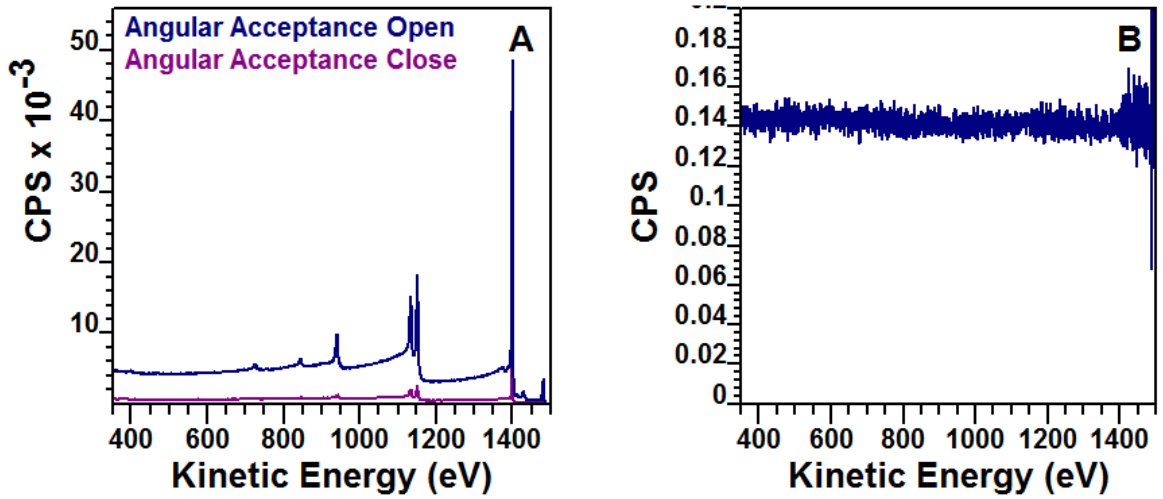

Figure 6. Comparison of angular acceptance PE 80eV Mode FOV2. A direct spectrum B Spectrum angular acceptance close divided by angular acceptance open

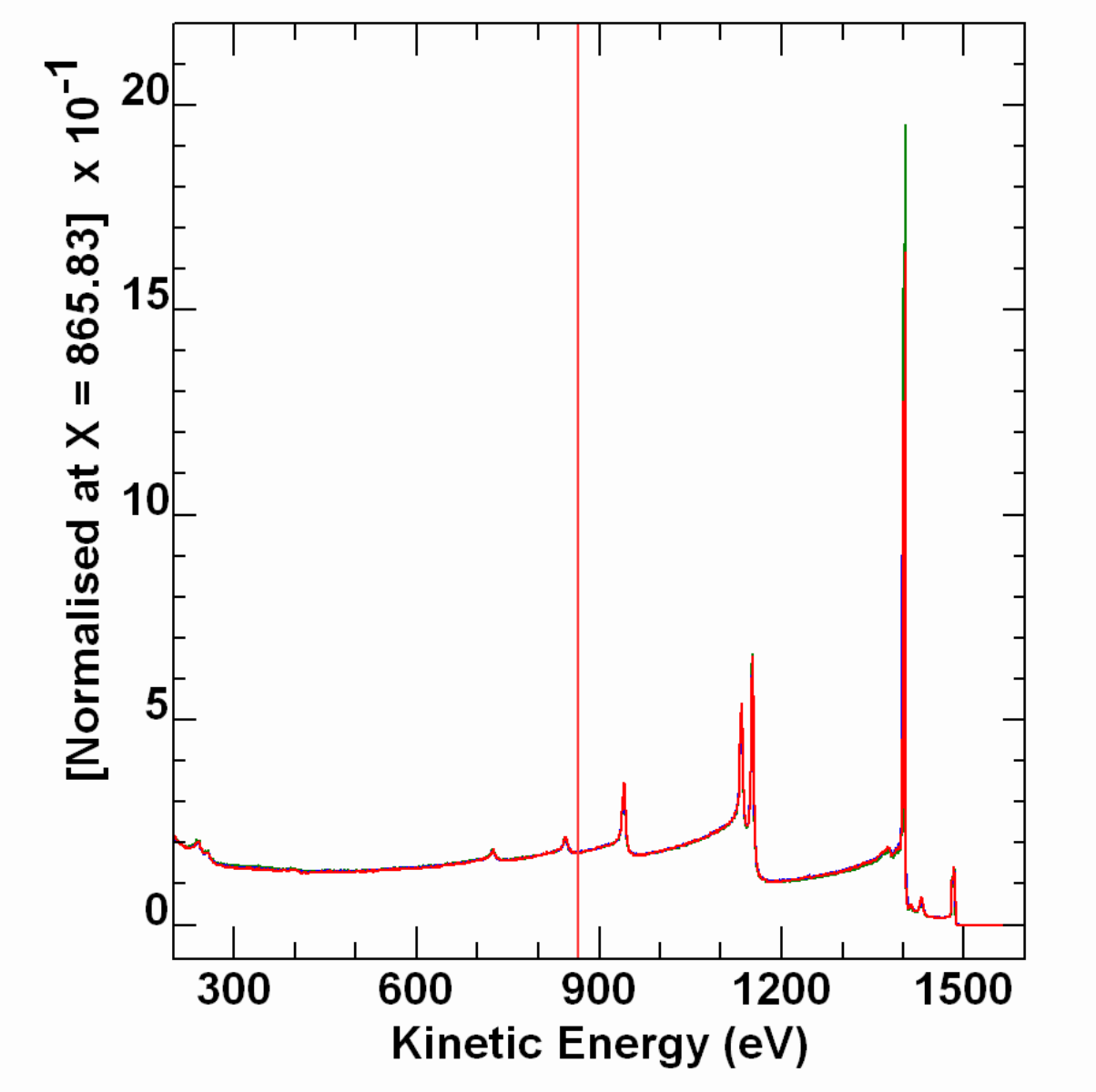

Figure 7: Gold survey spectra measured from the clean gold sample. Three spectra are overlaid including NPL transmission corrected Axis Ultra hybrid mode PE 80 eV from John Walton [11], Axis Nova FoV2 PE160 eV and FoV2 PE 80 eV.

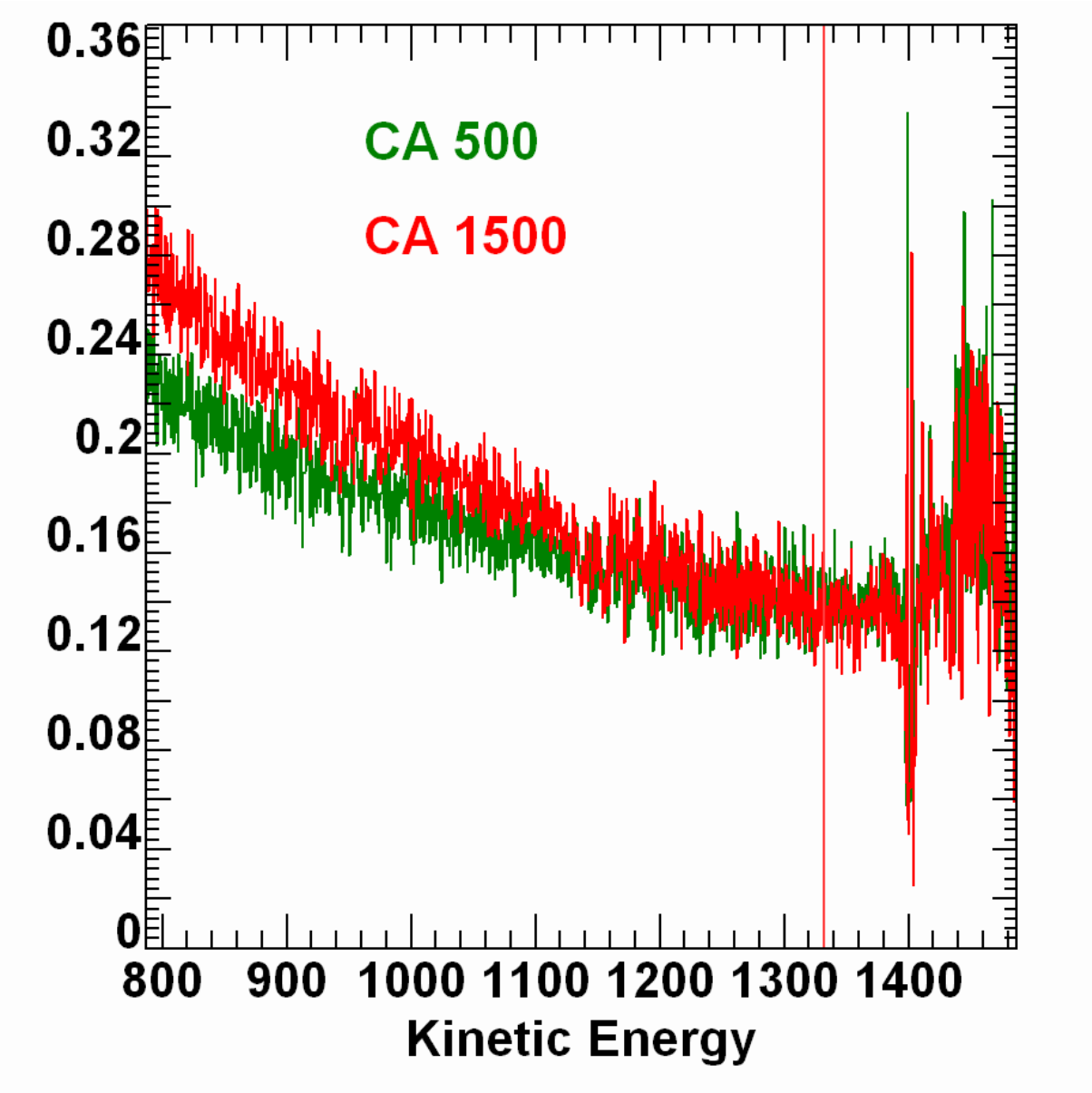

Figure 8. NanoESCA clean gold sample spectra relative to NPL true gold spectrum. Transmission for PE 50 CA 500 obeys an energy law of $E^{-0.9}$ while CA 1500 obeys $E^{-1.25}$.

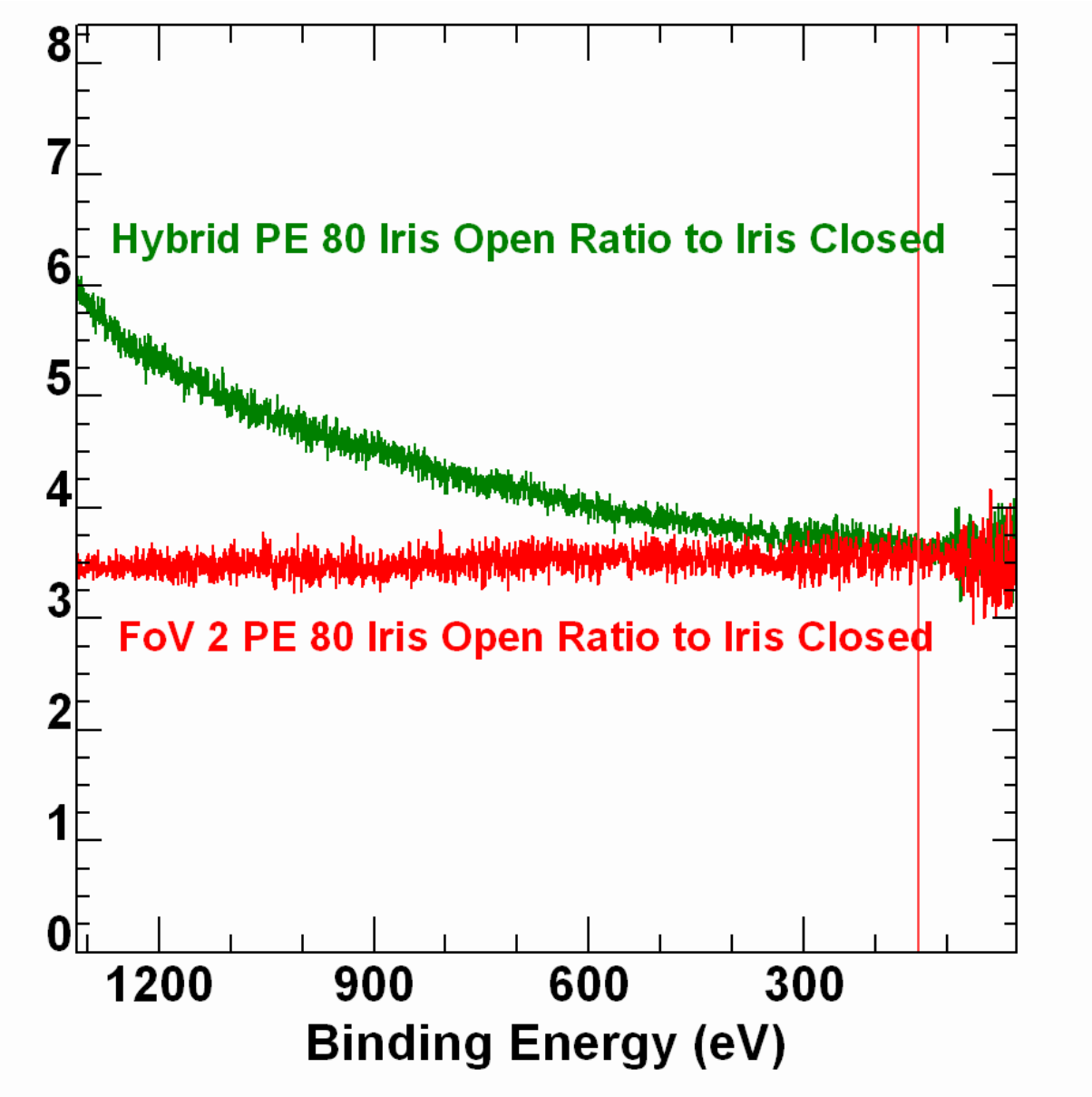

Figure 9. Axis Ultra gold spectrum was measured using PE 80 Hybrid and PE 80 FoV 2 measured using angular-acceptance iris fully open and fully closed. Spectra are displayed relative to the iris closed position for angular acceptance concerning each operating mode. Note FoV 2 shape is identical for angular acceptance iris open and closed. Closing the iris simply reduces sensitivity.

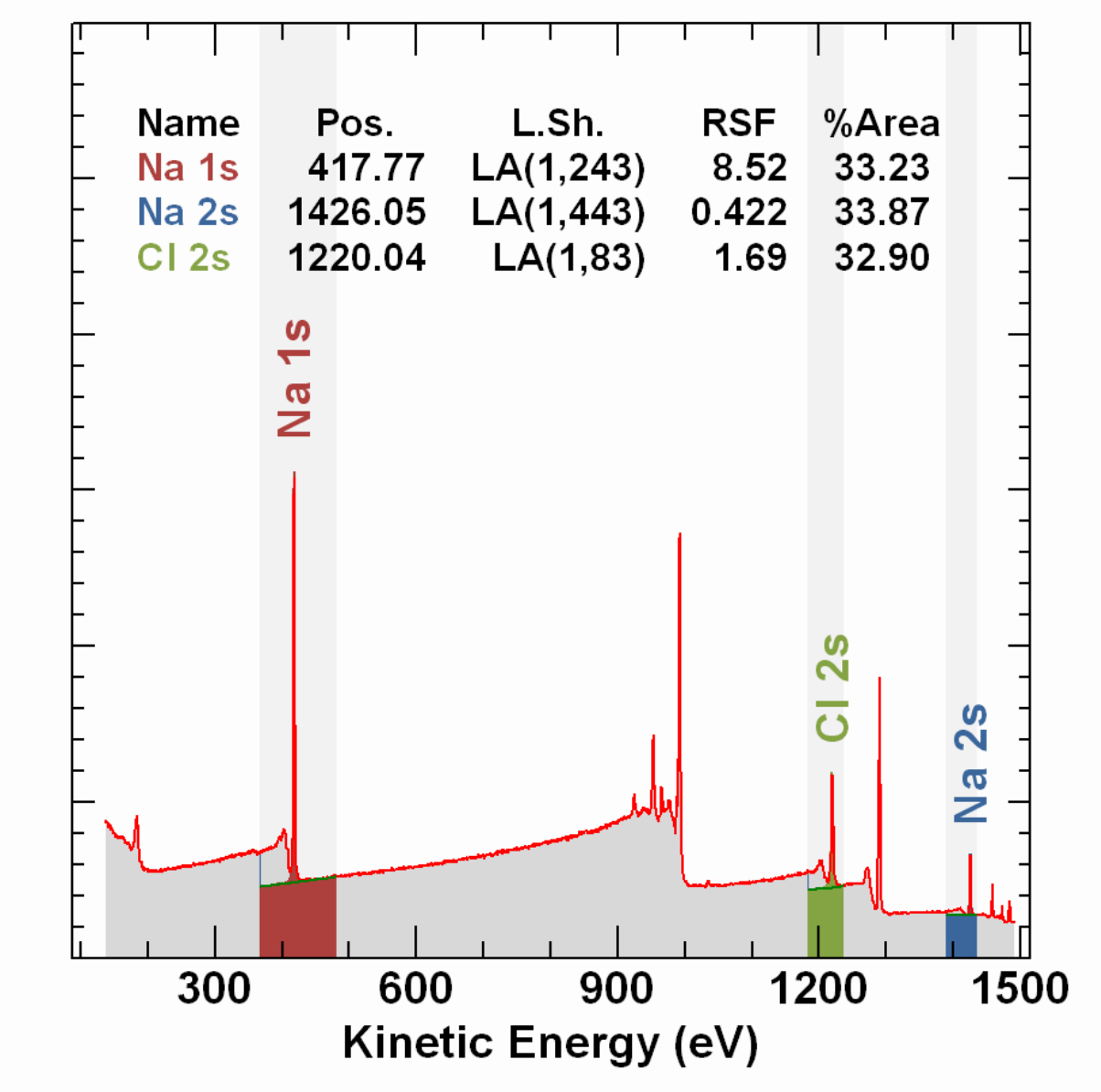

Figure 10: Quantification of Axis Nova FoV2 PE 160 spectrum measured from NaCl crystal. Photoemission intensities are measured by making use of Voigt line shapes and backgrounds extrapolated from signals with higher kinetic energy that the photoemission peak corresponds to Na 1s, Cl 2s and Na 2s. Scofield cross-sections were corrected for effective attenuation length escape depth correction and no transmission correction.

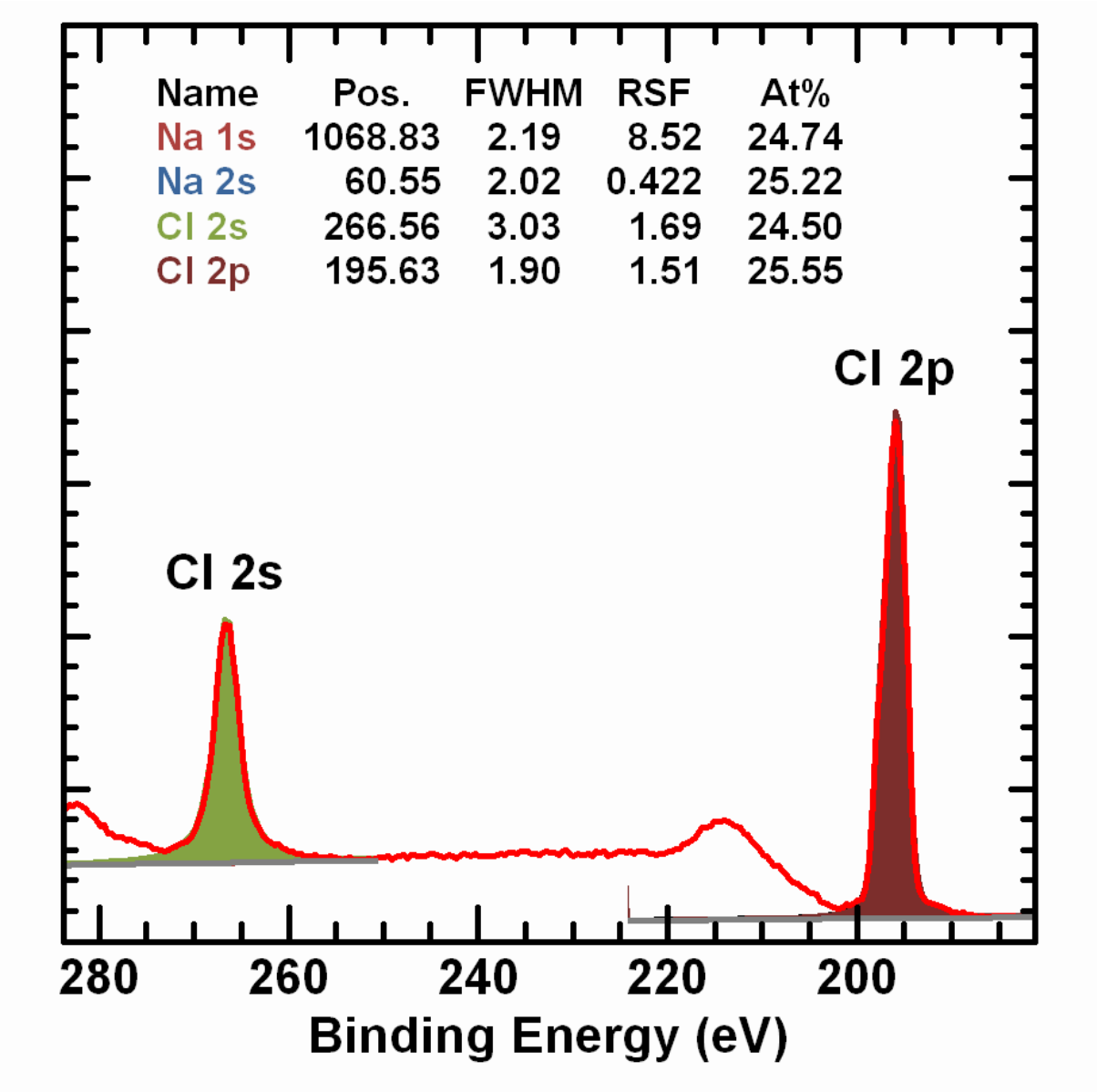

Figure 11: Cl 2s and Cl 2p photoemission from NaCl corrected using Scofield cross-sections and EAL.

References

[1] C. J. Powell, ‘Growth and trends in Auger-electron spectroscopy and x-ray photoelectron spectroscopy for surface analysis’, *Journal of Vacuum Science & Technology A*, vol. 21, no. 5, pp. S42–S53, Sep. 2003, doi: 10.1116/1.1599862.

[2] C. J. Powell and A. Jablonski, ‘Surface sensitivity of X-ray photoelectron spectroscopy’, *Nuclear Instruments and Methods in Physics Research Section A: Accelerators, Spectrometers, Detectors and Associated Equipment*, vol. 601, no. 1, pp. 54–65, Mar. 2009, doi: 10.1016/j.nima.2008.12.103.

[3] F. Reniers and C. Tewell, ‘New improvements in energy and spatial (x, y, z) resolution in AES and XPS applications’, *Journal of Electron Spectroscopy and Related Phenomena*, vol. 142, no. 1, pp. 1–25, Jan. 2005, doi: 10.1016/j.elspec.2004.07.004.

[4] M. P. Seah and G. C. Smith, ‘Quantitative AES and XPS: Determination of the electron spectrometer transmission function and the detector sensitivity energy dependencies for the production of true electron emission spectra in AES and XPS’, *Surf. Interface Anal.*, vol. 15, no. 12, pp. 751–766, Dec. 1990, doi: 10.1002/sia.740151208.

[5] P. J. Cumpson and M. P. Seah, ‘Random uncertainties in AES and XPS: II: Quantification using either relative or absolute measurements’, *Surface and Interface Analysis*, vol. 18, no. 5, pp. 361–367, May 1992, doi: 10.1002/sia.740180509.

[6] J. H. Scofield, ‘Hartree-Slater subshell photoionization cross-sections at 1254 and 1487 eV’, *Journal of Electron Spectroscopy and Related Phenomena*, vol. 8, no. 2, pp. 129–137, 1976, doi: 10.1016/0368-2048(76)80015-1.

[7] A. Jablonski and C. J. Powell, ‘Comparisons of practical attenuation lengths obtained from different algorithms for application in XPS’, *Surface Science*, vol. 520, no. 1, pp. 78–96, Nov. 2002, doi: 10.1016/S0039-6028(02)02267-7.

[8] Y. M. Cross and J. E. Castle, ‘The relationship between transmission efficiencies in the FRR and fat modes of an electron spectrometer’, *Journal of Electron Spectroscopy and Related Phenomena*, vol. 22, no. 1, pp. 53–60, Jan. 1981, doi: 10.1016/0368-2048(81)85004-9.

[9] A. G. Shard and S. J. Spencer, ‘Intensity calibration for monochromated Al Kα XPS instruments using polyethylene’, *Surface and Interface Analysis*, vol. 51, no. 6, pp. 618–626, Jun. 2019, doi: 10.1002/sia.6627.

[10] M. A. Mahjoub, G. Monier, C. Robert-Goumet, L. Bideux, and B. Gruzza, ‘New method for the determination of the correction function of a hemisperical electron analyser based on elastic electron images’, *Journal of Electron Spectroscopy and Related Phenomena*, vol. 197, pp. 80–87, Dec. 2014, doi: 10.1016/j.elspec.2014.09.010.

[11] J. Walton and N. Fairley, ‘A traceable quantification procedure for a multi-mode X-ray photoelectron spectrometer’, *Journal of Electron Spectroscopy and Related Phenomena*, vol. 150, no. 1, pp. 15–20, Jan. 2006, doi: 10.1016/j.elspec.2005.08.001.

[12] M. Holzweber, W. E. S. Unger, and V.-D. Hodoroaba, ‘Ionic Liquids as a Reference Material Candidate for the Quick Performance Check of Energy Dispersive X-ray Spectrometers for the Low Energy Range below 1 keV’, *Anal. Chem.*, vol. 88, no. 14, pp. 6967–6970, Jul. 2016, doi: 10.1021/acs.analchem.6b01444.

[13] K. Harrison and L. B. Hazell, ‘The determination of uncertainties in quantitative XPS/AES and its impact on data acquisition strategy’, *Surface and Interface Analysis*, vol. 18, no. 5, pp. 368–376, May 1992, doi: 10.1002/sia.740180510.

[14] D. A. Shirley, ‘High-Resolution X-Ray Photoemission Spectrum of the Valence Bands of Gold’, *Phys. Rev. B*, vol. 5, no. 12, pp. 4709–4714, Jun. 1972, doi: 10.1103/PhysRevB.5.4709.

[15] J. Végh, ‘The analytical form of the Shirley-type background’, *Journal of Electron Spectroscopy and Related Phenomena*, vol. 46, no. 2, pp. 411–417, Jan. 1988, doi: 10.1016/0368-2048(88)85038-2.

[16] M. P. Seah, I. S. Gilmore, and S. J. Spencer, ‘Background subtraction: II. General behaviour of REELS and the Tougaard universal cross section in the removal of

backgrounds in AES and XPS', *Surface Science*, vol. 461, no. 1, pp. 1–15, Aug. 2000, doi: 10.1016/S0039-6028(00)00373-3.
[17] I. W. Drummond, T. A. Cooper, and F. J. Street, 'Aspects of multidetector use in multitechnique surface analysis instrumentation', *Spectrochimica Acta Part B: Atomic Spectroscopy*, vol. 40, no. 5, pp. 773–779, Jan. 1985, doi: 10.1016/0584-8547(85)80128-2.
[18] M. Escher *et al.*, 'Nanoelectron spectroscopy for chemical analysis: a novel energy filter for imaging x-ray photoemission spectroscopy', *Journal of Physics: Condensed Matter*, vol. 17, no. 16, pp. S1329–S1338, Apr. 2005, doi: 10.1088/0953-8984/17/16/004.
[19] M. Escher *et al.*, 'NanoESCA: Imaging UPS and XPS with high energy resolution', *Journal of Electron Spectroscopy and Related Phenomena*, vol. 144–147, pp. 1179–1182, 2005, doi: 10.1016/j.elspec.2005.01.250.
[20] E. M. Purcell, 'The Focusing of Charged Particles by a Spherical Condenser', *Phys. Rev.*, vol. 54, no. 10, pp. 818–826, Nov. 1938, doi: 10.1103/PhysRev.54.818.
[21] D. Roy and D. Tremblay, 'Design of electron spectrometers', *Reports on Progress in Physics*, vol. 53, no. 12, pp. 1621–1674, Dec. 1990, doi: 10.1088/0034-4885/53/12/003.
[22] H. Z. Sar-El, 'More on the spherical condenser as an analyser I. Nonrelativistic part', *Nuclear Instruments and Methods*, vol. 42, no. 1, pp. 71–76, Jun. 1966, doi: 10.1016/0029-554X(66)90271-0.
[23] M. P. Seah, 'Simple universal curve for the energy-dependent electron attenuation length for all materials', *Surface and Interface Analysis*, vol. 44, no. 10, pp. 1353–1359, Oct. 2012, doi: 10.1002/sia.5033.
[24] Fairley, N., Fernandez, V., Richard-Plouet, M., Guillot-Deudon, C., Walton, J., Smith, E., Flahaut, D., Greiner, M., Biesinger, M., Tougaard, S., Morgan, D., and Baltrusaitis, J. (2021) Systematic and collaborative approach to problem solving using X-ray photoelectron spectroscopy. *Appl. Surf. Sci. Adv.*, **5**, 100112.
[25] Cumpson, P.J., Seah, M.P., and Spencer, S.J. (1998) The calibration of Auger and X-ray photoelectron spectrometers for valid analytical measurements. *Spectrosc. Eur.*, **10** (3), 8–15.